Anomalous thermoelectricity at the two-dimensional structural transition of SnSe monolayers

John W. Villanova and Salvador Barraza-Lopez

Phys. Rev. B **103**, 035421 — Published 21 January 2021

DOI: 10.1103/PhysRevB.103.035421

Anomalous thermoelectricity at the 2D structural transition of SnSe monolayers

John W. Villanova[1,*] and Salvador Barraza-Lopez[1,†]

[1] *Department of Physics, University of Arkansas, Fayetteville, AR 72701, USA*

The thermoelectric figure of merit ZT comprises electronic and vibrational contributions that change across phase transitions, and the most common theoretical *ab initio* approach to thermoelectricity fails to describe the evolution of ZT across finite-temperature structural transitions in its entirety. Furthermore, while the thermoelectric behavior of *bulk* SnSe has been extensively studied, SnSe *monolayers* have only been experimentally realized within this year, and the existent prediction of thermoelectricity on this two-dimensional material is unreliable because it misses its structural transition altogether. SnSe monolayers (and similar GeS, GeSe, SnS, and SnTe monolayers) experience a temperature induced two-dimensional $\mathrm{Pnm2_1} \rightarrow \mathrm{P4/nmm}$ structural transition precipitated by the softening of vibrational modes, and we describe its thermoelectric properties across the phase transition using molecular dynamics data to inform the thermoelectric coefficients directly. Similar to recent experimental observations pointing to an overestimated ZT past the transition temperature in bulk SnSe, we find a smaller ZT on SnSe monolayers when compared to its value predicted by the standard paradigm, due to the dramatic changes in the electrical conductivity and lattice thermal conductivity as the structural transition ensues. The process described here lends a strong focus to both the vibrational and electronic evolution throughout the structural transition, and it applies to thermoelectric materials undergoing thermally-driven solid-to-solid structural phase transitions in one, two, and three dimensions.

I. INTRODUCTION

The theory of thermoelectricity has clear mandates for improvement when the community observes that "finding ways to move beyond our current reliance on the ground state electronic and phonon band structures will be key to future progress in this area"[1]. Bulk SnSe has been argued to display an extremely large thermoelectric figure of merit ZT at its thermally-driven $\mathrm{Pnma} \rightarrow \mathrm{Cmcm}$ structural transition [2–7]. Nevertheless, the existence of such a high ZT has been put in doubt recently [8–10]: the lattice thermal conductivity (κ_l) appears to be seriously underestimated throughout the structural transition.

SnSe monolayers are structurally-stable binary semiconductors with an intrinsic in-plane electric dipole moment in their ground-state $\mathrm{Pnm2_1}$ structural configuration [11, 12]. While bulk SnSe undergoes a phase transition at temperatures as high as 900 K [13], SnSe monolayers on graphite display a critical temperature closer to 400 K [11]. A previous study of the thermoelectric properties of freestanding SnSe monolayers did not address the effect of the structural transition on thermoelectric properties [14]. Here, we discuss a process to capture the effects of phase transitions on thermoelectric properties.

The thermoelectric figure of merit is given by [1, 15]:

$$ZT = \frac{\sigma S^2 T}{\kappa_e + \kappa_l}, \tag{1}$$

where σ is the electrical conductivity, S is the Seebeck coefficient, T is the temperature, and κ_e is the electronic contribution to the thermal conductivity. We determine the thermoelectric figure of merit ZT across a thermally-driven structural phase transition relying directly on structural data obtained at finite-T. As a result, we predict a sudden increase in σ, κ_e, and κ_l across the structural transition [16, 17]. ZT decreases substantially near the onset of the structural transition. Our findings put to question record high values of ZT (in excess of 3 [14]) on materials undergoing structural phase transitions [9, 10]. Though exemplified in a two-dimensional (2D) ferroelectric, the process applies to any material undergoing solid-to-solid structural transitions.

II. METHODS

To this end, *ab initio* molecular dynamics (MD) calculations on (2D) SnSe monolayers employing the *SIESTA* code [18] were carried out on a $16 \times 16 \times 1$ supercell containing 1024 atoms within the isothermal-isobaric (NPT) ensemble. We captured dynamics over 28,000 fs for more than ten temperatures between 0 and 400 K with a 1.5 fs time resolution. The out-of-plane lattice vector had a length of 22 Å to ensure no interaction between periodic copies (see [12, 16, 17, 19–21] for additional details). For comparison purposes, the ShengBTE code [22] was used to calculate κ_l; the interatomic forces were calculated using the same settings employed in *SIESTA* on a $5 \times 5 \times 1$ supercell with up to third neighbors for the third-order force constants. We used a $36 \times 36 \times 1$ k-point mesh and a `scalebroad` parameter of 1.0. We took the average structure from each temperature in the MD calculation and used *SIESTA* to calculate Hamiltonian and overlap matrices. The electronic transport coefficients were obtained using Boltzmann transport theory [15, 22].

* jvillano@uark.edu
† sbarraza@uark.edu

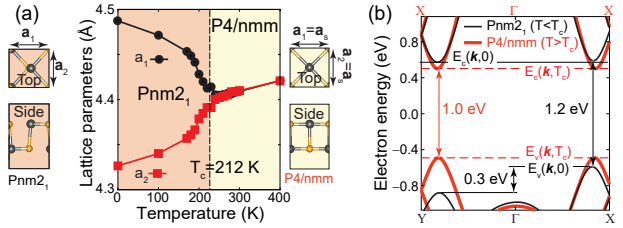

FIG. 1. (a) Thermal evolution of in-plane lattice parameters a_1 and a_2 for a freestanding SnSe monolayer, demonstrating a structural transition from an orthorhombic unit cell onto a unit cell with tetragonal symmetry at $T_c = 212$ K [16, 17]. Top and side views of the atomistic arrangements are shown, too. (b) Evolution of the valence (v) and conduction (c) bands of the SnSe monolayer as a result of the transition.

III. RESULTS AND DISCUSSION

Figure 1(a) displays the average lattice parameters a_1 and a_2 of a freestanding SnSe monolayer as a function of T. A fit of critical exponents yields $T_c = 212$ K [16]. The larger experimental value of 400 K [11] is attributed to the interaction of the SnSe monolayer with its supporting substrate. The SnSe monolayer turns paraelectric at $T \geq T_c$, as the unit cell develops a four-fold symmetry consistent with the P4/nmm space group. Fig. 1(a), experiment [11], and the fact that the standard thermoelectric theory relies on zero-temperature structural data, all demonstrate that an incorrect atomistic symmetry (Pnm2$_1$) has been previously employed to determine the thermoelectric properties of a SnSe monolayer within the reported 300-700 K temperature range [14, 23, 24].

Setting the focus on dimensionality aside for a moment, and giving context for our approach, two articles resemble the methodology proposed here. One is Ref. [6]. In that paper, the authors use a supercell with 256 atoms and the NVT ensemble. Their electronic contributions to ZT show a sharp discontinuity at 750 K (when pressure is 0 GPa) or at 500 K (when pressure is 4 GPa); this ensues because of the use of two atomistic structures (with either Pnma or Cmcm symmetry) to compute these quantities. While the electronic contributions to ZT are computed for up to 1,000 K, the lattice thermal conductivity is computed within a smaller (200 to 500 K) temperature range. No estimate of ZT is provided there. The second work is Ref. [7]. There, three structures are used to inform the Seebeck coefficient over a 900 K temperature range, and read directly from experimental data [13] at 298 K, 790 K, and 825 K.

The fact that only two references (out of so many devoted to bulk SnSe) discuss the effect of a changing atomistic structure on thermoelectric properties reinforces the observation that common paradigms are failing to describe the evolution of thermoelectric properties across phase transitions. The use of finite-T information straight from *ab initio* molecular dynamics to determine all thermoelectric properties is delineated next.

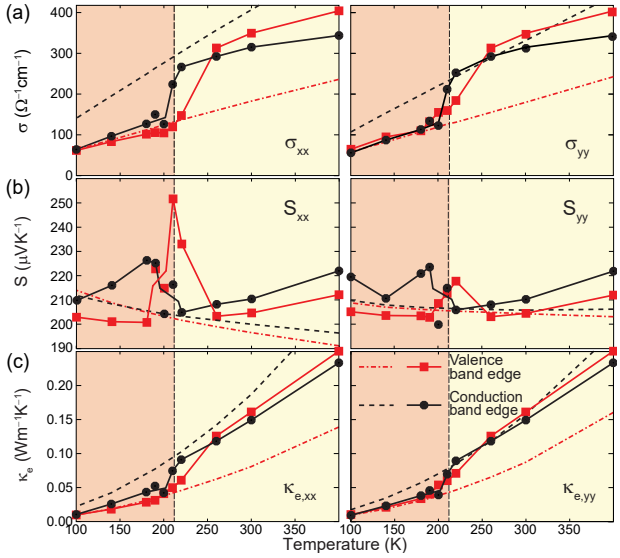

FIG. 2. (a) Electrical conductivity σ, (b) S, and (c) κ_e along the $\mathbf{a}_1$ (x) and $\mathbf{a}_2$ (y) directions versus T, respectively, for μ set at the conduction and valence band edges. Note the upticks at T_c due to a temperature-induced band alignment and the enhanced symmetry past T_c, both absent features in the standard approach (dashed and dash-dotted curves).

Structural changes modify the electronic bands: the electronic structure shown in black in Fig. 1(b) corresponds to the Pnm2$_1$ atomistic structure at $T = 0$; that is, to the electronic structure employed at all temperatures (300 to 700 K) in works that rely on the standard *ab initio* formalism for thermoelectricity (*e.g.*, Refs. [14, 23, 24] for the SnSe monolayer at hand). The electronic bands shown in red in Figure 1(b) correspond to the average atomistic structure of the freestanding SnSe monolayer above 212 K. The two hole valleys turn degenerate due to the enhanced tetragonal symmetry of the P4/nmm space symmetry group. In what follows, the electronic band structure is labeled $E_\alpha(\mathbf{k}, T)$, where α is the band index, to emphasize its dependency on the average unit cell at finite-T.

The temperature dependence of σ in the standard *ab initio* approach to thermoelectricity only enters through a scattering time τ and through the Fermi-Dirac distribution $f(E-\mu, T)$. Here however, σ_{ij} incorporates the finite-T dependency of the electron group velocities and of the unit cell area as well [1]:

$$\sigma_{ij}(T) = \frac{e^2}{\Omega(T)} \sum_{\mathbf{k},\alpha} \mathrm{v}_{\alpha,i}(\mathbf{k}, T)\mathrm{v}_{\alpha,j}(\mathbf{k}, T)\tau_e(T)g(E, \mu, T), \tag{2}$$

where $g(E, \mu, T) = -\frac{\partial f(E-\mu,T)}{\partial E}$, $i = x, y$ and $j = x, y$ represent cartesian coordinates, e is the electron charge, and $\hbar$ is the reduced Planck constant. $\Omega(T)$ is the T-dependent volume of the unit cell, τ_e is the electron relax-

ation time, $\mathrm{v}_{\alpha,i}(\mathbf{k},T)=\frac{1}{\hbar}\frac{\partial E_\alpha(\mathbf{k},T)}{\partial k_i}$ is the band group velocity. Although the electron relaxation time τ_e may also be T-dependent, a T-independent magnitude of 10^{-14} s is assigned in accordance with previous estimates [4, 14, 24–26].

Figure 2(a) showcases in dashed (dashed-dotted) lines the electron (hole) conductivity with μ at the conduction (valence) band edge using a zero-T relaxed volume and zero-T electronic structure to compare the prediction of this new method with the standard paradigm. The T-dependent method deployed here, shown by solid lines and red squares (black circles) for the valence (conduction) band edge, tracks closely with the standard paradigm for $T<T_c$. However, there is a marked increase in the σ at T_c as the electron (hole) pockets of the conduction (valence) band align due to an increased symmetry above T_c. For $T>T_c$, the standard paradigm predicts greater electron conductivity as compared to hole conductivity, but our T-dependent formalism indicates the opposite trend for $T\geq 250$ K. (Work on bulk SnSe displays a similar increase in carrier concentration (electrical conductivity) induced by the transition [2, 7], but the observed behavior of σ was assigned to the creation of Sn vacancies [7], as opposed to the band alignment due to symmetry showcased in Fig. 1(b).)

We next account for the Seebeck coefficient S, obtained by dividing the expression

$$[\sigma S(T,\mu)]_{ij}=\frac{-e}{T\Omega(T)}\times \tag{3}$$
$$\sum_{\mathbf{k},\alpha}\mathrm{v}_{\alpha,i}(\mathbf{k},T)\mathrm{v}_{\alpha,j}(\mathbf{k},T)\tau_e g(E,\mu,T)(E_\alpha(\mathbf{k},T)-\mu)$$

by Eqn. (2). S, as depicted in Figure 2(b), was computed with μ set at either the valence or conduction band edges. As it was the case for σ, S is asymmetric in the usual formalism. It exhibits a peak at T_c for S_{xx}, and a subdued peak for S_{yy}. When contrasted with the temperature evolution of σ, S is otherwise roughly constant over the temperature range investigated, showing an increase and a subsequent decrease as in bulk samples [7, 13].

The denominator in Eqn. (1) contains the electronic and lattice contributions to the thermal conductivity. The $\kappa_{e,ij}$ tensor has two terms,

$$\kappa_{e,ij}(T,\mu)=\mathcal{K}_{ij}(T,\mu)-T[\sigma S(T,\mu)]^2_{ij}\sigma(T,\mu)^{-1}_{ij}, \tag{4}$$

with the first contribution being

$$\mathcal{K}_{ij}(T,\mu)=\frac{1}{T\Omega(T)}\times \tag{5}$$
$$\sum_{\mathbf{k},\alpha}\mathrm{v}_{\alpha,i}(\mathbf{k},T)\mathrm{v}_{\alpha,j}(\mathbf{k},T)\tau_e g(E,\mu,T)(E_\alpha(\mathbf{k},T)-\mu)^2,$$

and the second term expressible from Eqns. (2) and (3). κ_e [Fig. 2(c)] displays a trend similar to the one observed for σ in Fig. 2(a). Transport coefficients turn symmetric past T_c, which could serve as an experimental signature to verify whether this finite-T approach to thermoelectricity surpasses the state-of-the-art. Calculating κ_l requires additional methods to collect phonon frequencies and lifetimes from the MD data, which we present next.

In materials at the onset of structural transitions,[27–29] "anharmonicity drives the crystal past the zero-temperature structure onto a new crystalline phase for which the zero-temperature electronic and zero-temperature phonon dispersions may no longer carry meaning" [30]. There have been vigorous efforts to account for temperature-dependent effects on ZT[31–34], yet most *ab initio* thermoelectricity works ignore structural transitions altogether [1, 15, 22, 35]; and these modifications have certainly not been employed to discuss 2D thermoelectrics yet. Here, the challenge is met by using the power spectrum of the vibrational modes derived from molecular dynamics by way of the velocity autocorrelation function.

Fig. 3(a) displays the first Brillouin zone and the $k-$point sampling achieved with a 16×16 supercell without interpolation [36]. The high-T phase is fourfold-symmetric [17], making the $X-$ and $Y-$points equivalent. A power spectrum at each $k-$point is obtained by Fourier transforming the velocities of the atoms into reciprocal space, performing the time autocorrelation, and then Fourier transforming into frequency space [37]. This process yields the resonant natural frequencies $\nu_\alpha(\mathbf{k},T)$ demonstrated at two nearby $k-$points $\mathbf{k}$ at $T=100$ K and 230 K in Fig. 3(b).

The finite-T phonon dispersions of the freestanding SnSe monolayer along the red path in Fig. 3(a) are shown in Fig. 3(c). The central frequencies $\nu_\alpha(\mathbf{k},T)$ and the full width at half-max $\Delta\nu_\alpha(\mathbf{k},T)$ were fitted to Lorentzian functions at each $k-$point and T; phonon lifetimes are given by $\tau_{l,\alpha}(\mathbf{k},T)=(\pi\Delta\nu_\alpha(\mathbf{k},T))^{-1}$. The average value of $\tau_{l,\alpha}(\mathbf{k},T)$ was 2.6 ps across the 100 to 400 K temperature range studied here, and we observe a softening of vibrational modes along the Brillouin zone boundary at frequencies between 2 and 4 THz for $T>T_c$ [17] in Figs. 3(b) and 3(c).

The power spectra data describe the vibrational frequencies at each temperature and includes information on phonon-phonon interactions through broadening of the natural frequencies. This *non-perturbative* process fully incorporates anharmonicity in the phonon frequencies and phonon lifetimes, in contrast to the standard approach [22] whereby phonon scattering rates are determined self-consistently in a perturbation series and added together. Furthermore, the phonon spectrum in Fig. 3(c) reflects the structural transition [16, 17, 21, 29] shown earlier in Fig. 1. These non-perturbative finite-T vibrational modes profoundly affect ZT.

Obtaining the lattice thermal conductivity κ_l [Fig. 3(d)] requires the phonon group velocity $v_{\alpha,i}(\mathbf{k},T)$ (with $i=x,y$), calculated by finite-differences for the α-th mode at each $k-$point and T. This way, κ_l is given

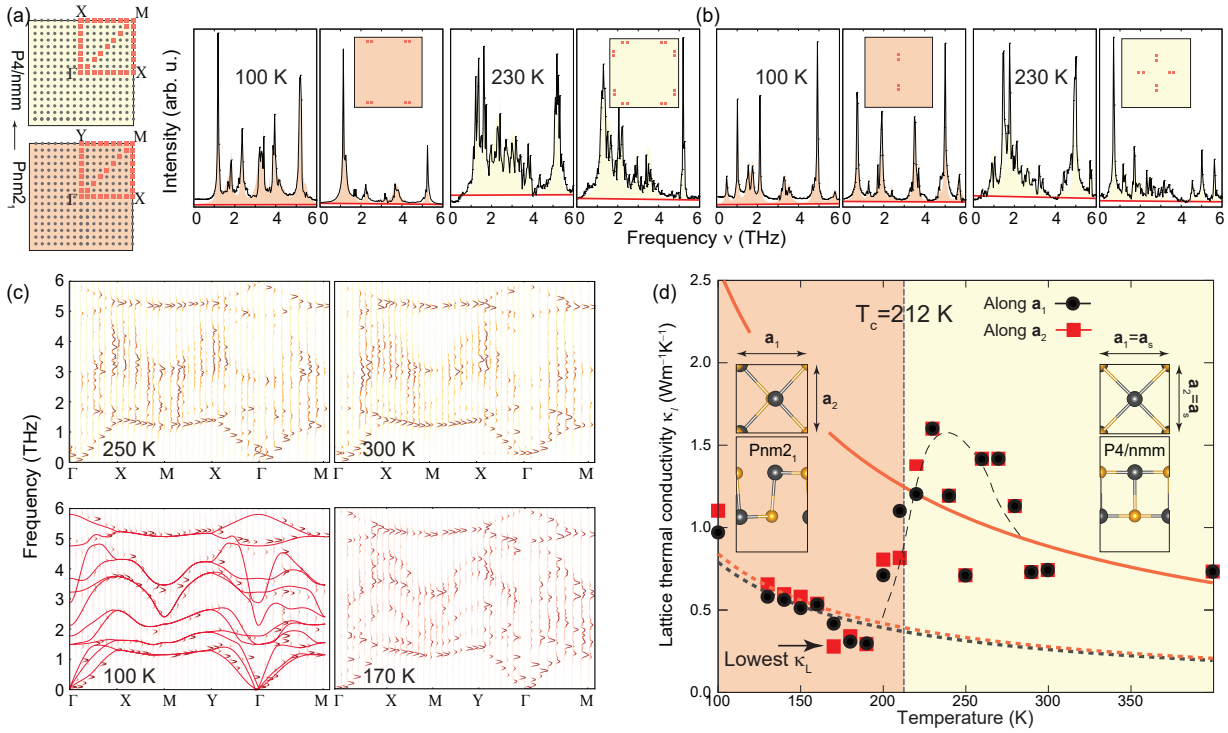

FIG. 3. (a) First Brillouin zone above (top) and below T_c (bottom) [16, 17]. (b) Power spectra at two consecutive $k-$points. (c) Phonon spectrum for T above T_c (top subplots) and below T_c (lower subplots) along the red path in (a). Optical phonon modes with frequencies between 2 to 4 THz soften at $T > T_c$. Red curves are zero-T phonons as a guide to the eye. (d) κ_l from the phonon spectrum at finite-T along the $x-$ (a_1, circles) and $y-$ (a_2, squares) directions. The solid line is the fit to the data above $T = 190$ K and the dotted black (red) line is the fit to the data below $T = 190$ K along the a_1 (a_2) direction. The black dashed curve is a guide to the eye showing the sudden increase in κ_l at and beyond T_c.

by:

$$\kappa_{l,ij}(T) = \frac{1}{\Omega(T)} \times \sum_{\mathbf{k},\alpha} v_{\alpha,i}(\mathbf{k},T) v_{\alpha,j}(\mathbf{k},T) \tau_{l,\alpha}(\mathbf{k},T) C_{ph,\alpha}(\mathbf{k},T), \tag{6}$$

with $\tau_{l,\alpha}(\mathbf{k},T)$ the phonon lifetime and $C_{ph,\alpha}(\mathbf{k},T)$ the mode-dependent heat capacity,

$$C_{ph,\alpha}(\mathbf{k},T) = k_B \left(\frac{h\nu_\alpha(\mathbf{k},T)}{k_B T}\right)^2 \frac{e^{h\nu_\alpha(\mathbf{k},T)/k_B T}}{(e^{h\nu_\alpha(\mathbf{k},T)/k_B T} - 1)^2}. \tag{7}$$

Even though C_{ph} is expressed within the harmonic approximation, the velocities and frequencies are obtained from MD and are thus "renormalized" in the sense that they include anharmonic contributions by design.

The peak shown in Fig. 3(d) near the transition temperature is reminiscent of the anomalous lattice thermal conductivity experimentally observed in $SmBaMn_2O_6$ single crystals across their structural transition [38]. Here, in the ferroelectric $Pnm2_1$ phase below $T_c = 212$ K, κ_l decreases with a $\propto T^{-1}$ behavior. The lattice thermal conductivity is comparable with κ_e close to T_c, at which point κ_l exhibits a sudden increase across and above the transition temperature. A study of Cu_2Se, Cu_2S, Ag_2S, and Ag_2Se indicated a substantially reduced lattice thermal conductivity just before the onset of their T-dependent phase transition [9]. In agreement with Ref. [10], we find a larger κ_l past T_c than the usual method, which ignores the transition altogether.

Optical phonons have been found to contribute to κ_l substantially [39–41]; in other monochalcogenide systems the contribution owing to the optical modes can be greater than 20% of the total κ_l [42], and it can be as high as 30% in bulk SnSe [43]. Even just on the basis of Eqn. (6), the unmitigated increase in the phonon velocities, lifetimes, and softened frequencies dominates the lattice thermal conductivity despite a saturating heat capacity C_{ph}. An enhanced κ_l has been attributed to higher velocity softened phonon modes both in silica [44] and in double-perovskite $SmBaMn_2O_6$ single crystals [38], too.

ZT is determined along the $x-$ and $y-$directions in Fig. 4 for both fixed electron or hole densities and for carrier densities such that μ maximizes ZT at each temperature. $ZT_{xx} \neq ZT_{yy}$ for all T within the standard approach to thermoelectricity, due to the use of the rectangular ground state atomistic structure at all temperatures. Using the finite-T data, the thermoelectric figure of merit ZT is similar to predictions based on zero-

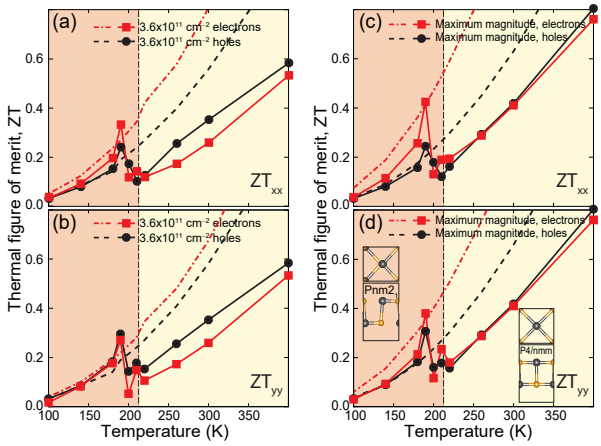

FIG. 4. Thermoelectric figure of merit ZT for the freestanding SnSe monolayer as a function of T for electron (hole) doping in red rectangles (black circles) within the method presented here. Predictions from the standard method are shown by dashed-dotted (dashed) curves for electrons (holes). (a) ZT along the $x-$direction and (b) along the $y-$direction for a fixed carrier density of 3.6×10^{11} cm^{-2}. (c) ZT along the $x-$direction and (d) along the $y-$direction for a varying level of doping which maximizes ZT. Note the decreased magnitude of ZT past T_c in contrast to the standard paradigm.

temperature data for T <180 K. ZT displays a significant and symmetric drop beyond 190 K, a result in conflict with previous reports on SnSe monolayers in which the structural transition is ignored and which overestimate ZT [14, 23, 24]. The apparent spike in ZT near T_c is similar to the behavior observed in iodine-doped or alloyed bulk Cu_2Se [45–47].

IV. CONCLUSION

In conclusion, we investigated the thermoelectric behavior of a prototypical SnSe monolayer across its two-dimensional ferroelectric-to-paraelectric phase transition, incorporating finite-T MD data to inform both the electronic and the lattice thermal behavior. We demonstrate that the standard approach to thermoelectricity overestimates ZT for this 2D material, and introduce a method to predict the dramatic effect of the T-dependent structural phase transition on ZT that applies to arbitrary thermoelectric materials undergoing solid-to-solid phase transitions.

The authors were funded by an Early Career Award from the U.S. DOE (DE-SC0016139). Calculations were performed at NERSC, a U.S. DOE User Facility (DE-AC02-05CH11231).

[1] A. Zevalkink, D. M. Smiadak, J. L. Blackburn, A. J. Ferguson, M. L. Chabinyc, O. Delaire, J. Wang, K. Kovnir, J. Martin, L. T. Schelhas, T. D. Sparks, S. D. Kang, M. T. Dylla, G. J. Snyder, B. R. Ortiz, and E. S. Toberer, A Practical Field Guide to Thermoelectrics: Fundamentals, Synthesis, and Characterization, Appl. Phys. Rev. **5**, 021303 (2018).

[2] L.-D. Zhao, S.-H. Lo, Y. Zhang, H. Sun, G. Tan, C. Uher, C. Wolverton, V. P. Dravid, and M. G. Kanatzidis, Ultralow thermal conductivity and high thermoelectric figure of merit in SnSe crystals, Nature **508**, 373 (2014).

[3] C. Chang, M. Wu, D. He, Y. Pei, C.-F. Wu, X. Wu, H. Yu, F. Zhu, K. Wang, Y. Chen, L. Huang, J.-F. Li, J. He, and L.-D. Zhao, 3d charge and 2d phonon transports leading to high out-of-plane zt in n-type snse crystals, Science **360**, 778 (2018).

[4] G. Ding, G. Gao, and K. Yao, High-efficient thermoelectric materials: The case of orthorhombic IV-VI compounds, Sci. Rep. **5**, 9567 (2015).

[5] R. Guo, X. Wang, Y. Kuang, and B. Huang, First-principles study of anisotropic thermoelectric transport properties of iv-vi semiconductor compounds snse and sns, Phys. Rev. B **92**, 115202 (2015).

[6] H. Yu, S. Dai, and Y. Chen, Enhanced power factor via the control of structural phase transition in snse, Sci. Rep. **6**, 26193 (2016).

[7] A. Dewandre, O. Hellman, S. Bhattacharya, A. H. Romero, G. K. H. Madsen, and M. J. Verstraete, Two-step phase transition in snse and the origins of its high power factor from first principles, Phys. Rev. Lett. **117**, 276601 (2016).

[8] P.-C. Wei, S. Bhattacharya, Y.-F. Liu, F. Liu, J. He, Y.-H. Tung, C.-C. Yang, C.-R. Hsing, D.-L. Nguyen, C.-M. Wei, M.-Y. Chou, Y.-C. Lai, T.-L. Hung, S.-Y. Guan, C.-S. Chang, H.-J. Wu, C.-H. Lee, W.-H. Li, R. P. Hermann, Y.-Y. Chen, and A. M. Rao, Thermoelectric figure-of-merit of fully dense single-crystalline snse, ACS Omega **4**, 5442 (2019).

[9] H. Chen, Z. Yue, D. Ren, H. Zeng, T. Wei, K. Zhao, R. Yang, P. Qiu, L. Chen, and X. Shi, Thermal Conductivity during Phase Transitions, Adv. Mater. **31**, 1806518 (2019).

[10] M. T. Agne, P. W. Voorhees, and G. J. Snyder, Phase Transformation Contributions to Heat Capacity and Impact on Thermal Diffusivity, Thermal Conductivity, and Thermoelectric Performance, Adv. Mater. **31**, 1902980 (2019).

[11] K. Chang, F. Küster, B. J. Miller, J.-R. Ji, J.-L. Zhang, P. Sessi, S. Barraza-Lopez, and S. S. P. Parkin, Microscopic manipulation of ferroelectric domains in snse monolayers at room temperature, Nano Lett. **20**, 6590 (2020).

[12] S. Barraza-Lopez, B. M. Fregoso, J. W. Villanova, S. S. P. Parkin, and K. Chang, Colloquium: Physical behavior of group-IV monochalcogenide monolayers, (accepted for publication at Reviews of Modern Physics) arXiv:2009.04341.

[13] T. Chattopadhyay, J. Pannetier, and H. Von Schnering, Neutron Diffraction Study of the Structural Phase Transition in SnS and SnSe, J. Phys. Chem. Solids **47**, 879 (1986).

[14] F. Q. Wang, S. Zhang, J. Yu, and Q. Wang, Thermoelec-

tric properties of single-layered SnSe sheet, Nanoscale **7**, 15962 (2015).
[15] G. K. Madsen and D. J. Singh, BoltzTraP. A code for calculating band-structure dependent quantities, Comput. Phys. Commun. **175**, 67 (2006).
[16] S. Barraza-Lopez, T. P. Kaloni, S. P. Poudel, and P. Kumar, Tuning the Ferroelectric-to-Paraelectric Transition Temperature and Dipole Orientation of Group-IV Monochalcogenide Monolayers, Phys. Rev. B **97**, 024110 (2018).
[17] J. W. Villanova, P. Kumar, and S. Barraza-Lopez, Theory of finite-temperature two-dimensional structural transformations in group-iv monochalcogenide monolayers, Phys. Rev. B **101**, 184101 (2020).
[18] J. M. Soler, E. Artacho, J. D. Gale, A. García, J. Junquera, P. Ordejón, and D. Sánchez-Portal, The SIESTA Method for Ab Initio Order-N Materials Simulation, J. Phys.: Condens. Matter **14**, 2745 (2002).
[19] M. Mehboudi, A. M. Dorio, W. Zhu, A. van der Zande, H. O. H. Churchill, A. A. Pacheco-Sanjuan, E. O. Harriss, P. Kumar, and S. Barraza-Lopez, Two-Dimensional Disorder in Black Phosphorus and Monochalcogenide Monolayers, Nano Lett. **16**, 1704 (2016).
[20] M. Mehboudi, B. M. Fregoso, Y. Yang, W. Zhu, A. van der Zande, J. Ferrer, L. Bellaiche, P. Kumar, and S. Barraza-Lopez, Structural Phase Transition and Material Properties of Few-Layer Monochalcogenides, Phys. Rev. Lett. **117**, 246802 (2016).
[21] S. P. Poudel, J. W. Villanova, and S. Barraza-Lopez, Group-IV monochalcogenide monolayers: Two-dimensional ferroelectrics with weak intralayer bonds and a phosphorenelike monolayer dissociation energy, Phys. Rev. Materials **3**, 124004 (2019).
[22] W. Li, J. Carrete, N. A. Katcho, and N. Mingo, ShengBTE: A solver of the Boltzmann transport equation for phonons, Comput. Phys. Commun. **185**, 1747 (2014).
[23] Y. Sun, Z. Shuai, and D. Wang, Reducing Lattice Thermal Conductivity of the Thermoelectric SnSe Monolayer: Role of PhononElectron Coupling, J. Phys. Chem. C **123**, 12001 (2019).
[24] G. Ding, Y. Hu, D. Li, and X. Wang, A comparative study of thermoelectric properties between bulk and monolayer SnSe, Results Phys. **15**, 102631 (2019).
[25] Z.-Y. Hu, K.-Y. Li, Y. Lu, Y. Huang, and X.-H. Shao, High thermoelectric performances of monolayer SnSe allotropes, Nanoscale **9**, 16093 (2017).
[26] R. L. Gonzlez-Romero, A. Antonelli, and J. J. Melndez, Insights into the thermoelectric properties of SnSe from ab initio calculations, Phys. Chem. Chem. Phys. **19**, 12804 (2017).
[27] C. W. Li, J. Hong, A. F. May, D. Bansal, S. Chi, T. Hong, G. Ehlers, and O. Delaire, Orbitally driven giant phonon anharmonicity in SnSe, Nat. Phys. **11**, 1063 (2015).
[28] C. Chang, G. Tan, J. He, M. G. Kanatzidis, and L.-D. Zhao, The Thermoelectric Properties of SnSe Continue to Surprise: Extraordinary Electron and Phonon Transport, Chem. Mater. **30**, 7355 (2018).
[29] K. Chang, J. Liu, H. Lin, N. Wang, K. Zhao, A. Zhang, F. Jin, Y. Zhong, X. Hu, W. Duan, Q. Zhang, L. Fu, Q.-K. Xue, X. Chen, and S.-H. Ji, Discovery of robust in-plane ferroelectricity in atomic-thick snte, Science **353**, 274 (2016).
[30] J. Heremans, The anharmonicity blacksmith, Nature Phys. **11**, 990 (2015).
[31] P. Souvatzis, O. Eriksson, M. I. Katsnelson, and S. P. Rudin, Entropy driven stabilization of energetically unstable crystal structures explained from first principles theory, Phys. Rev. Lett. **100**, 095901 (2008).
[32] O. Hellman, A. Abrikosov, and S. I. Simak, Lattice dynamics of anharmonic solids from first principles, Phys. Rev. B **84**, 180301(R) (2011).
[33] A. H. Romero, E. K. U. Gross, M. J. Verstraete, and O. Hellman, Thermal conductivity in pbte from first principles, Phys. Rev. B **91**, 214310 (2015).
[34] N. Shulumba, O. Hellman, and A. J. Minnich, Lattice thermal conductivity of polyethylene molecular crystals from first-principles including nuclear quantum effects, Phys. Rev. Lett. **119**, 185901 (2017).
[35] A. J. H. McGaughey, A. Jain, H.-Y. Kim, and B. Fu, Phonon properties and thermal conductivity from first principles, lattice dynamics, and the Boltzmann transport equation, J. Appl. Phys. **125**, 011101 (2019).
[36] R. M. Pick, M. H. Cohen, and R. M. Martin, Microscopic theory of force constants in the adiabatic approximation, Phys. Rev. B **1**, 910 (1970).
[37] E. N. Koukaras, G. Kalosakas, C. Galiotis, and K. Papagelis, Phonon Properties of Graphene Derived From Molecular Dynamics Simulations, Sci. Rep. **5**, 12923 (2015).
[38] L. Chen, Z. Xiang, C. Tinsman, Q. Huang, K. G. Reynolds, H. Zhou, and L. Li, Anomalous thermal conductivity across the structural transition in SmBaMn2O6 single crystals, Appl. Phys. Lett. **114**, 251904 (2019).
[39] T. Shiga, J. Shiomi, J. Ma, O. Delaire, T. Radzynski, A. Lusakowski, K. Esfarjani, and G. Chen, Microscopic mechanism of low thermal conductivity in lead telluride, Phys. Rev. B **85**, 155203 (2012).
[40] T. Beechem, J. C. Duda, P. E. Hopkins, and P. M. Norris, Contribution of optical phonons to thermal boundary conductance, Appl. Phys. Lett. **97**, 061907 (2010).
[41] Z. Tian, K. Esfarjani, J. Shiomi, A. S. Henry, and G. Chen, On the importance of optical phonons to thermal conductivity in nanostructures, Appl. Phys. Lett. **99**, 053122 (2011).
[42] N. Shulumba, O. Hellman, and A. J. Minnich, Intrinsic localized mode and low thermal conductivity of PbSe, Phys. Rev. B **95**, 014302 (2017).
[43] G. Qin, Z. Qin, W.-Z. Fang, L.-C. Zhang, S.-Y. Yue, Q.-B. Yan, M. Hu, and G. Su, Diverse anisotropy of phonon transport in two-dimensional group IVVI compounds: A comparative study, Nanoscale **8**, 11306 (2016).
[44] H. Aramberri, R. Rurali, and J. Íñiguez, Thermal conductivity changes across a structural phase transition: The case of high-pressure silica, Phys. Rev. B **96**, 195201 (2017).
[45] H. Liu, X. Yuan, P. Lu, X. Shi, F. Xu, Y. He, Y. Tang, S. Bai, W. Zhang, L. Chen, Y. Lin, L. Shi, H. Lin, X. Gao, X. Zhang, H. Chi, and C. Uher, Ultrahigh Thermoelectric Performance by Electron and Phonon Critical Scattering in $Cu_2Se_{1-x}I_x$, Adv. Mater. **25**, 6607 (2013).
[46] D. Byeon, R. Sobota, K. Delime-Codrin, S. Choi, K. Hirata, M. Adachi, M. Kiyama, T. Matsuura, Y. Yamamoto, M. Matsunami, and T. Takeuchi, Discovery of colossal Seebeck effect in metallic Cu_2Se, Nature Commun. **10**, 72 (2019).
[47] D. Vasilevskiy, M. K. Keshavarz, J.-M. Simard, R. A. Masut, S. Turenne, and G. J. Snyder, Assessing the

Thermal Conductivity of $Cu_{2-x}Se$ Alloys Undergoing a Phase Transition via the Simultaneous Measurement of Thermoelectric Parameters by a Harman-Based Setup, J. Electron. Mater. **47**, 3314 (2018).